Open-Circuit Fault Diagnosis for the Grid-Tied T-Type Inverter Based Only on Three-Phase Currents

Zhixi WU and Jin ZHAO

***Abstract*—Grid-tied T-type inverters are widely used in photovoltaic, electric vehicle charging piles, and other grid-tied applications. However, the transistor fault seriously harms the reliability of the inverter. This paper proposed a simple and novel open-circuit fault diagnosis method for the grid-tied T-type inverter based only on the three-phase currents. At first, the Hausdorff distances among the three-phase normalized current accumulations are obtained to perform the fault detection. The process is tolerant of inverter transient conditions. Then, the fundamental frequency values of the three-phase currents are calculated to locate the faulty phase. At last, the faulty transistor is located by some intermediate conditions. In particular, the method is suitable for modulation index regulation. Experiments verify the effectiveness of the proposed method.**

***Index Terms*—Fundamental frequency value, grid-tied T-type inverter, Hausdorff distance, open-circuit fault diagnosis, three-phase currents.**

I. Introduction

MULTI-LEVEL inverters are widely used in grid-tied energy conversion systems (such as photovoltaic, electric vehicle charging piles, and wind turbines), because of their higher efficiency, less current harmonics, lower overall costs, and inherent fault-tolerance, compared to two-level converters [1], [2]. Among the many types of multi-level inverters (such as T-type, NPC, NPP, and so on), the T-type inverter performs well in the application of medium switching frequency and tens kilowatt so that it is a kind of crucial grid-tied inverter [3], [4].

Transistor fault seriously harms the reliability of the system, causing energy loss and even system shutdown [5]. Unfortunately, transistors are none other than fragile components in converters. Around 38% of the faults in power systems are due to semiconductor devices [6]. From an industrial perspective [7], 40% of the attention should be on semiconductor devices to improve the reliability of the power system. The T-type inverter has twice as many transistors as the two-level converter, so it faces a greater risk of transistor fault.

Manuscript received March 8, 2024; revised June 3, 2024; accepted June 20, 2024. Date of publication September 30, 2024; date of current version July 16, 2024. This work was supported in part by the China National Science Foundation under Grants 62073147 and 61573159. *(Corresponding author: Jin zhao.)*

Both authors are with the School of Artificial Intelligence and Automation, Huazhong University of Science and Technology, Wuhan 430074, China (e-mail: wzx_@hust.edu.cn; jinzhao617@ hust.edu.cn).

Digital Object Identifier 10.24295/CPSSTPEA.2024.00012

The transistor fault types include short-circuit faults and open-circuit faults. Hardware protection circuits often deal with instantaneous overvoltage and overcurrent caused by the short-circuit fault. Open-circuit fault results in output distortion and harmonics, which becomes the major concern of transistor faults [8]. The open-circuit fault diagnosis method can quickly locate the fault transistor, provide the basis for fault tolerant control or maintenance decisions, and greatly improve the system's reliability.

Recently, much research on open-circuit fault diagnosis has been carried out, which can be simply classified as model-based methods, data-based methods, and signal-based methods. Model-based methods collect system parameters and build accurate circuit models to estimate the residuals, to realize fault diagnosis. Data-based methods mine fault information from a large number of system data by techniques of machine learning or deep learning and obtain fault results by classifiers. Signal-based methods use the voltage or current signals of the system to obtain fault information through signal analysis and processing.

Compared with signal-based methods and data-based methods, model-based methods typically require more types of system parameters. In the case of two-level power converters, models such as the pole-to-pole model [9] and phase voltage model [10] are used to realize fault diagnosis. When applying these models, it is necessary to obtain system parameters such as voltages, currents, inductances and capacitances, or currents and switching states. In the case of multi-level power converters, the models built are more complex and there are more fault states. The average voltage model is built to design fault diagnosis methods for T-type inverters [11], which solve the disturbance caused by working conditions in multi-level converters, such as modulation index regulation. A kind of node-path model and the voltage model are used to diagnose the single open-circuit fault for the T-type inverter [12]. In NPC rectifier fault diagnosis, the line voltage model is built to obtain the error value, and then the diagnosis method is designed based on the error [13]. The two diagnosis methods realize the diagnostic speed of switching period levels because of the combination of switching states. Model-based methods are quick to diagnose and adapt to complex working conditions. However, many system parameters are usually required, and these parameters may not be available or accurate, which may limit the application of model-based methods.

Data-based methods are more used in fault diagnosis of two-

level converters [14], [15]. There is also precedent for the data-based method in NPC converter [16]. However, it is rarely reported in the diagnosis of T-type converters. Although many of the data-based methods only need to collect a single type of system signal as the input of the learning models, the training of the models needs a lot of training samples. This requires a lot of data acquisition work, and the high computational complexity also increases the difficulty of application.

Signal-based methods have also been widely studied in recent years. In the case of two-level converters, there are many diagnostic methods based only on the three-phase currents [17], [18]. In [19], line voltages are analyzed and used to design the diagnosis method. These methods require only one kind of system signal and are more applicable. Unfortunately, existing signal-based methods in multilevel converter diagnosis still use more system signals or control operations. In the fault diagnosis for grid-tied NPC inverters, the three-phase currents are used as the diagnostic signals, and additional operations such as the underexcited power injection and the switching scheme are performed separately to locate the fault [20], [21]. [22] designs the diagnosis method based on the three-phase currents and grid voltage angle for the T-type rectifier. However, the method is only effective for some transistors. In T-type inverters, [23] uses single-phase line voltage for fault diagnosis, but the performance under modulation index regulation and load regulation is not reported. [24] proposes a fast diagnosis method, but it is based on an additional neutral-point current sensor, three-phase currents, and switching states. In [25], the three-phase currents and two DC-bus capacitor voltages are used to diagnose the open-circuit fault.

In general, fewer diagnostic signals are used in diagnosis methods in favor of their application. There have been many researches and applications on the design of two-level converters using only three-phase currents. However, diagnosis methods for multilevel inverters such as T-type still usually use relatively more diagnostic signals or control operations. This paper proposes an online open-circuit fault diagnosis for the grid-tied T-type inverter based on only three-phase currents. Firstly, the fault mechanism of the inverter is analyzed in detail. Then, the design of the proposed method is given, which consists of three steps. The first step is to obtain the Hausdorff distances among the three-phase normalized current accumulations to perform the fault detection. The second step process is to calculate the fundamental frequency values of the three-phase currents to locate the faulty phase. The third step is to locate the faulty transistor by some intermediate conditions. Finally, simulations and experiments verify the robustness and effectiveness of the proposed method. The contributions are:

1) A novel online diagnosis method for the grid-tied T-type inverter only based on the three-phase currents is proposed. The Hausdorff distances and the fundamental frequency values are used as diagnosis features.
2) The proposed method is suitable for all single transistor open-circuit faults, considering modulation index regulation. The fault diagnosis is tolerant of inverter transient conditions.

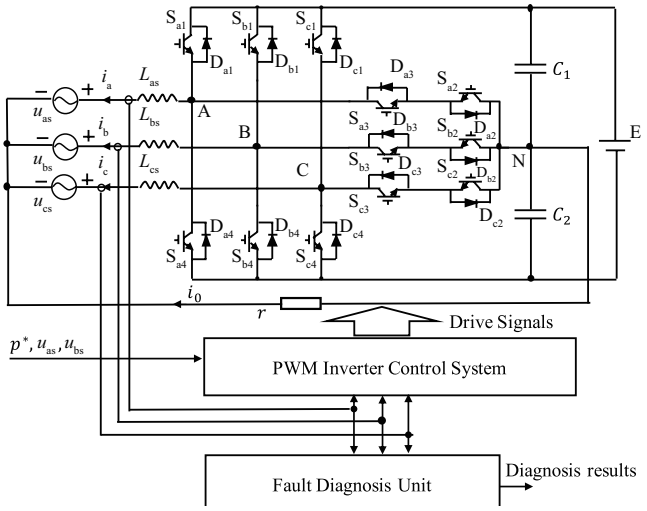

Fig. 1. The structure of the grid-tied T-type inverter with the proposed diagnosis unit.

TABLE I
THE SWITCHING STATE AND THE SWITCH COMBINATION

Switching state	The switch combination
P	S_{x1} and S_{x3} turn on, S_{x2} and S_{x4} turn off
O	S_{x2} and S_{x3} turn on, S_{x1} and S_{x4} turn off
N	S_{x2} and S_{x4} turn on, S_{x1} and S_{x3} turn off

Section II introduces the system of the grid-tied T-type inverter with the diagnosis unit. Section III is the analysis of the open-circuit fault mechanism in detail. Section IV introduces the design of the proposed method. Section V shows the simulations and experimental verifications. Section VI is the conclusion of this paper.

II. System of the Grid-Tied T-Type Inverter

As a multi-level converter, the grid-tied T-type inverter has a more complex topology than the two-level converter, as shown in Fig. 1. There are twelve transistors (S_{x1}, S_{x2}, S_{x3}, S_{x4}) and their respective fly-wheel diodes (D_{x1}, D_{x2}, D_{x3}, D_{x4}). x represents the three phases a, b, c. X represents the three phases A, B, C. N is the neutral point. u_{xs} are the three-phase grid voltages. L_{xs} represent filter inductances. i_x are the three-phase currents. The positive directions of i_x and u_{xs} are defined in Fig. 1. C_1 and C_2 are DC bus capacitances. E is the DC power supply. r and i_0 are neutral resistance and current. The PWM inverter control system collects i_x and u_{xs}, and then outputs the three-phase modulated voltage signals u_x according to the given power p^*. Drive signals can be calculated by u_x. When $u_x > 0$, there are switching states P and O in the x phase. When $u_x < 0$, there are switching states N and O in the x phase. The relationship between the switching state and the switch combination is shown in Table I. The proposed fault diagnosis unit only collects i_x to perform the fault diagnosis, without any other system signals (system parameters, control parameters, or other

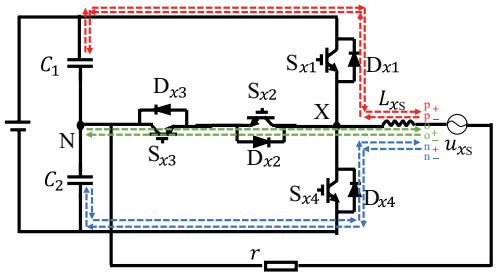

Fig. 2. The current paths under different switching states, considering the direction of the current.

electrical signals).

III. The Fault Mechanism Analysis

When analyzing the open-circuit fault mechanism, the working mode of the T-type inverter should be analyzed first. The inverter has three switching states (P, O, N). Considering the current direction, there are six current flow paths, as shown in Fig. 2. They are p_+ ($C_1 \rightarrow S_{x1} \rightarrow L_{xs} \rightarrow u_{xs}$), p_- ($u_{xs} \rightarrow L_{xs} \rightarrow D_1 \rightarrow C_1$), o_+ ($S_{x3} \rightarrow D_{x2} \rightarrow L_{xs} \rightarrow u_{xs}$), o_-($u_{xs} \rightarrow L_{xs} \rightarrow S_{x2} \rightarrow D_{x3}$), n_+ ($C_2 \rightarrow D_{x4} \rightarrow L_{xs} \rightarrow u_{xs}$), and n_- ($u_{xs} \rightarrow L_{xs} \rightarrow S_{x4} \rightarrow C_2$). In path p_-, o_-, and n_-, the current direction is negative. In paths p_+, o_+, and n_+, the current direction is positive. In paths p_- and p_+, the switching state is P. In paths o_- and o_+, the switching state is O. In paths n_-, and n_+, the switching state is N.

During the healthy operation of the inverter, the energy is transferred from the DC side to the grid side, which means that both i_x, and u_{xs} are in the positive direction. The pole-to-pole voltage U_{XN} is determined by the switching state and the capacitor voltages. The relationship between i_x and U_{XN} is shown in Fig. 3. The fault mechanisms of the current path under the health condition, the S_{x4} fault condition, and the S_{x2} fault condition are analyzed below. The S_{x1} fault condition and the S_{x3} fault condition are similar to the previous two fault conditions, except that the direction of each parameter is opposite.

A. The Health Condition

As shown in Fig. 3(a), path o_- and n_- exist in the negative current period. The power sources in n_- are C_2 and u_{xs}. The power sources in o_- is u_{xs}. n_- increases the amplitude of i_x, and o_- decreases it. The controller makes the current approximately sinusoidal by controlling the action time of the two paths.

B. The S_{x4} Fault Condition

When S_{x4} is faulty, path n_- cannot be conducted, which distorts the current in the negative period as shown in Fig. 3(b). Assuming the negative current exists, path p_- will replace the original path n_- to act, resulting in a decrease in the negative current. Path o_- does the same thing. So there is no negative current. In particular, the switch state O turns on both S_{x3} and S_{x2}. Under the action of u_{xs}, the amplitude of the positive current will increase in the O state. The presence of the positive current initiates paths p_+ and o_+. o_+ increases the amplitude of the positive current, but p_+ decreases it.

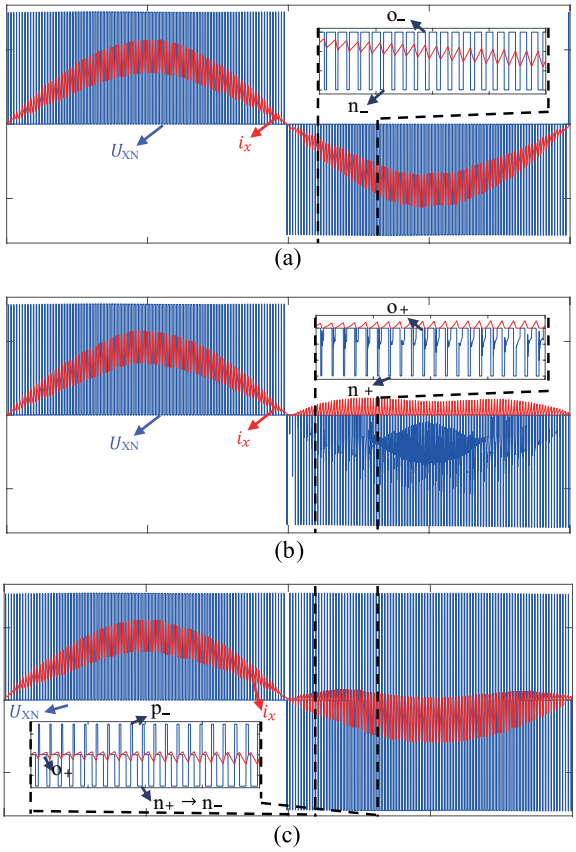

Fig. 3. Relationships between i_x and U_{XN} under (a) health, (b) S_{x4} fault and (c) S_{x2} fault.

C. The S_{x2} Fault Condition

When S_{x2} is faulty, path o_- cannot be conducted, which distorts the current in the negative period as shown in Fig. 3(c). The current distortion in S_{x2} fault is similar to that in S_{x4} fault, but it has a more complex distortion mode. Assuming the negative current exists, path p_- will replace the original path o_- to act, resulting in a decrease in the negative current. The action can be severe, resulting in zero amplitude of the negative current. In particular, the switch state O also turns on S_{x3}, making the presence of the positive current with path o_+. Switching state N conducts path n_+ and path n_- to decrease the positive current amplitude and increase the negative current amplitude, respectively. With the increase of the amplitude of u_x, the amplitude of the negative current increases, and the amplitude of the positive current decreases sharply.

From the above analysis, it can be obtained that the current will be distorted in the negative period under S_{x2} fault and S_{x4} fault. Only the positive current exists in the distortion period under S_{x4} fault. The proportion of negative current is higher than that of positive current in the distortion period under S_{x2} fault.

IV. Design of the Proposed Method

Only the three-phase currents are used to design the open-circuit diagnosis method in this paper. The method is a step-by-

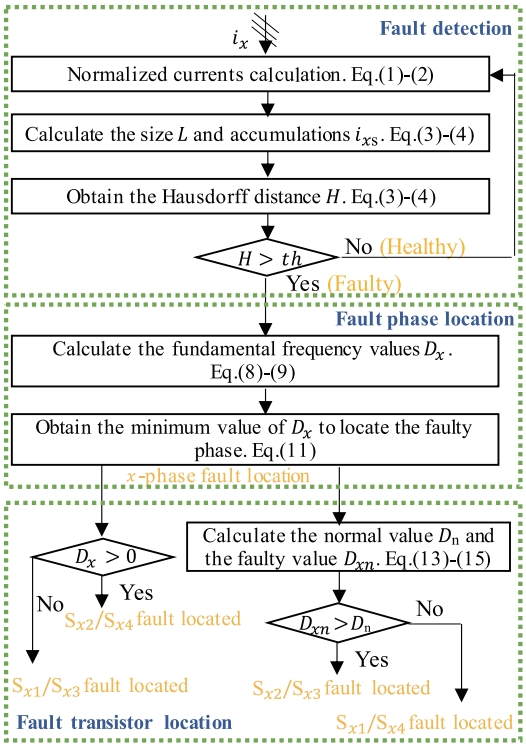

Fig. 4. The flowchart of the proposed diagnosis method.

step process. The first step is to obtain the Hausdorff distances among the three-phase normalized current accumulations to perform the fault detection. The second step process is to calculate the fundamental frequency values of the three-phase currents to locate the faulty phase. The third step is to locate the faulty transistor. The S_{x1}/S_{x3} or S_{x2}/S_{x4} fault is located by the three-phase normalized current accumulations and the S_{x2}/S_{x3} or S_{x1}/S_{x4} fault is located by the fundamental frequency values between the phases.

A. Fault Detection

To adapt to the effect of load and other changes on the three-phase currents, the current normalization operation is applied. In the healthy condition, the phase difference between the three currents is 120°. Let I_m be the peak value of currents. i_d, i_q and i_m are the intermediate variables. (1) can be obtained as:

$$\begin{cases} i_d = \sqrt{\frac{2}{3}}\, i_a - \sqrt{\frac{1}{6}}\, i_b = \sqrt{\frac{1}{6}}\, i_c \\ i_q = \sqrt{\frac{1}{2}}\, i_b - \sqrt{\frac{1}{2}}\, i_c \\ i_m = \sqrt{\frac{2}{3}(i_d^2 + i_q^2)} = I_m \end{cases} \tag{1}$$

The normalized currents $\bar{i_x}$ can be calculated as:

$$\bar{i_x} = \frac{i_x}{I_m} \tag{2}$$

Let the grid frequency be f_s and the current sampling frequency of the fault diagnosis unit be f. Define the size of the sliding window per unit current period to be L, and L can be calculated as (3). $\bar{i}_{xj}$ is the j-th sampling point of $\bar{i}_x$ in the window.

$$L = \frac{f}{f_s} \tag{3}$$

As analyzed in Section III, transistor fault will cause current distortion in positive or negative periods. The steady-state current is sinusoidal under healthy conditions. Therefore, the three-phase normalized current accumulations i_{xs} can be used to indicate the current distortion:

$$i_{xs} = \sum_{j=1}^{L} \bar{i}_{xj} \tag{4}$$

The Hausdorff distances among i_{xs} are defined in a sliding window of length $2L$. i_{xsj} is the j-th sampling point of i_{xs} in the window. The maximum value $i_{xs}^{\max}$ and the minimum value $i_{xs}^{\min}$ of the i_{xs} points in the sliding window should be obtained:

$$\begin{cases} i_{xs}^{\max} = \max\,(i_{xs1}, i_{xs2}, \ldots, i_{xs2L}) \\ i_{xs}^{\min} = \min\,(i_{xs1}, i_{xs2}, \ldots, i_{xs2L}) \end{cases} \tag{5}$$

The Hausdorff distances can be defined as:

$$\begin{cases} H_{ab} = \max\left[\max\,(i_{as}^{\min} - i_{bs}^{\max}, 0), \max\,(i_{bs}^{\min} - i_{as}^{\max}, 0)\right] \\ H_{bc} = \max\left[\max\,(i_{bs}^{\min} - i_{cs}^{\max}, 0), \max\,(i_{cs}^{\min} - i_{bs}^{\max}, 0)\right] \\ H_{ca} = \max\left[\max\,(i_{cs}^{\min} - i_{as}^{\max}, 0), \max\,(i_{as}^{\min} - i_{cs}^{\max}, 0)\right] \\ H = \mathrm{mid}\,(H_{ab}, H_{bc}, H_{ca}) \end{cases} \tag{6}$$

The Hausdorff distance is symmetric, meaning that $H_{ab} = H_{ba}$, $H_{bc} = H_{cb}$, and $H_{ac} = H_{ca}$. In the healthy condition, H is close to zero. In the faulty condition, H is a positive value. The current accumulation calculated for an ideal half-period normalized current is $\sum_{j=1}^{L} \left|\sin\left(\frac{2\pi j}{L}\right)\right|/2$. Therefore, the fault detection function can be to determine whether H exceeds threshold th, whose value is $k\sum_{j=1}^{L} \left|\sin\left(\frac{2\pi j}{L}\right)\right|/2$. (0.2, 0.5) is considered as the value range of k. The fault detection function is

$$\begin{cases} H > th, \text{ faulty condition} \\ H \leqslant th, \text{ healthy condition} \end{cases} \tag{7}$$

B. Fault Phase Location

Fault phase location is performed after an open-circuit fault is detected. The fundamental frequency values D_x of i_x are used as fault features. Let i_{xj} is the j-th sampling point of i_x in the sliding window. Define $D_x^{\sin}$ and $D_x^{\cos}$ to be the sine and cosine components of D_x, respectively. $D_x^{\sin}$, $D_x^{\cos}$ and D_x can be calculated as (8), (9) and (10), respectively.

$$D_x^{\sin} = \sum_{j=1}^{L} \left[i_{xj} \sin\left(\frac{2\pi j}{L}\right)/L \right] \tag{8}$$

$$D_x^{\cos} = \sum_{j=1}^{L}\left[i_{xj}\cos\left(\frac{2\pi j}{L}\right)/L\right] \tag{9}$$

$$D_x = \sqrt{D_x^{\sin}\cdot D_x^{\sin} + D_x^{\cos}\cdot D_x^{\cos}} \tag{10}$$

The calculation of D_x is independent of the start of the sliding window and is easy to perform online. Because of the current distortion, the fundamental frequency of the fault phase is smaller than that of the other two phases. Therefore, the fault phase location function is

$$D_x = \min(D_a, D_b, D_c),\ x-\text{phase fault} \tag{11}$$

C. S_{x1}/S_{x3} or S_{x2}/S_{x4} Fault Location

After the phase location, the x-phase fault is obtained, and then S_{x1}/S_{x3} or S_{x2}/S_{x4} fault location is performed. As analyzed in Section III, the current distortion caused by S_{x1}/S_{x3} occurs in the positive period of the current, and the current distortion caused by S_{x2}/S_{x4} occurs in the negative period of the current. The distortion in the negative period will cause the positive current accumulation to be greater than the negative current accumulation. In the same way, the distortion in the positive period will cause the negative current accumulation to be greater than the positive current accumulation. Therefore, the defined i_{xs} can perform this location process as shown in (12).

$$\begin{cases} i_{xs} > 0,\ \mathbf{S}_{x2}/\mathbf{S}_{x4}\ \text{fault is located} \\ i_{xs} < 0,\ \mathbf{S}_{x1}/\mathbf{S}_{x3}\ \text{fault is located} \end{cases} \tag{12}$$

D. S_{x1}/S_{x4} or S_{x2}/S_{x3} Fault Location

According to the analysis in Section III, the current distortions under S_{x1} fault and S_{x3} are similar, and the same is true between S_{x2} fault and S_{x4}. However, the proportions of positive current and negative current in the distortion period are important features for similarity discrimination, which are reflected in the fundamental frequency values D_x. With x-phase S_{x1}/S_{x4} fault, D_x will be reduced and less than half of the normal fundamental frequency value. With x-phase S_{x2}/S_{x3} fault, D_x will be reduced but greater than half of the normal fundamental frequency value. Half of the normal fundamental frequency value D_n can be calculated in real time using the fundamental frequency value $D_n^{\max}$ obtained from the other two healthy phases within a sliding window L, as shown in (13) and (14). $D_{nj}^{\max}$ is the j-th sampling point of $D_n^{\max}$ in the window. k_1 is a threshold with a value range of (1.05, 1.1) to resist the adverse effects of noise on the location.

$$D_n^{\max} = [(D_a + D_b + D_c) - \min(D_a, D_b, D_c)]/4 \tag{13}$$

$$D_n = k_1 \max(D_{n1}^{\max}, D_{n2}^{\max}, \ldots, D_{nL}^{\max}) \tag{14}$$

The last location process can be performed as (15) and (16). D_{xj} is the j-th sampling point of D_x in the sliding window. Finally, the faulty transistor can be diagnosed.

$$D_{xn} = \min(D_{x1}, D_{x2}, \ldots, D_{xL}) \tag{15}$$

$$\begin{cases} D_{xn} > D_n,\ \mathbf{S}_{x2}/\mathbf{S}_{x3}\ \text{fault is located} \\ D_{xn} < D_n,\ \mathbf{S}_{x1}/\mathbf{S}_{x4}\ \text{fault is located} \end{cases} \tag{16}$$

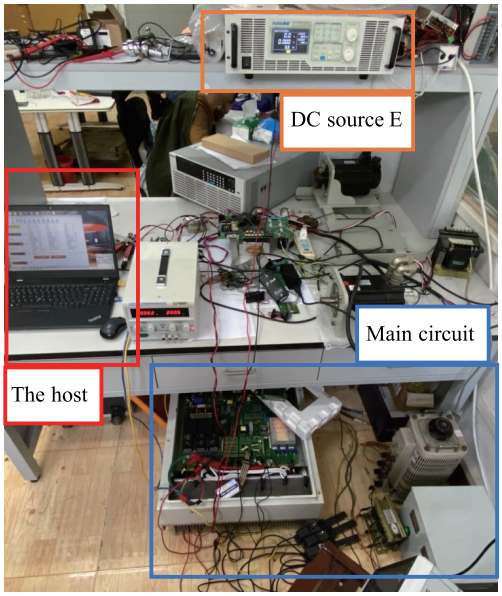

Fig. 5. The experimental platform used for verification.

A flowchart of the proposed diagnosis method is given as shown in Fig. 4, which consists of the fault detection, fault phase location, and fault transistor location. The diagnosis results are obtained in the corresponding steps.

V. Experimental Verification

The experimental platform used for verification is shown in Fig. 5. The main circuit uses 10-FY12NMA160SH01 IGBT modules and a TMS320F28335 controller. DC source is FTG100-800. The current sampling frequency f is 5 kHz. The grid source frequency f_s is 50 Hz and RMS is 50 V. The switching frequency f_k is 10 kHz, and the dead time t_d is 2 μs. The capacitances C_1 and C_2 are both 550 μF, and the filter inductances L_{xs} are all 2.632 mH. The open-circuit fault is realized by the host shielding the driver signal. The thresholds k and k_1 are set to 0.3 and 1.08, respectively. The experiments verify the robustness and effectiveness of fault diagnosis under the modulation index regulation.

A. Transient Performance Verification

The start-up process, DC side voltage changing, and output power adjustment are the most common working transient conditions of the inverter. The fault diagnosis unit should not be triggered by mistake under these conditions. The performance of the proposed method under the transient conditions is evaluated below.

Fig. 6 shows the performance verification in the start-up process. The three-phase currents fluctuate caused of the grid voltages before the action of the driven signals. The current normalization operation limits the three-phase current to the unit range. When the driven signals are applied, the currents have a large response, which causes the abrupt change of i_{xs}. However, the Hausdorff distance H is significantly reduced, which avoids the false trigger.

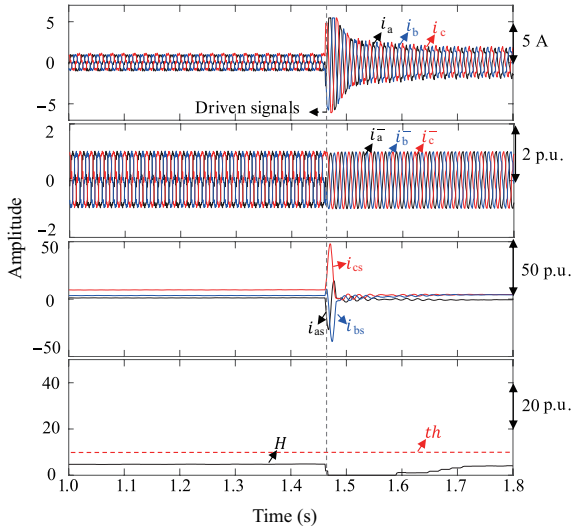

Fig. 6. Experimental results in the start-up process.

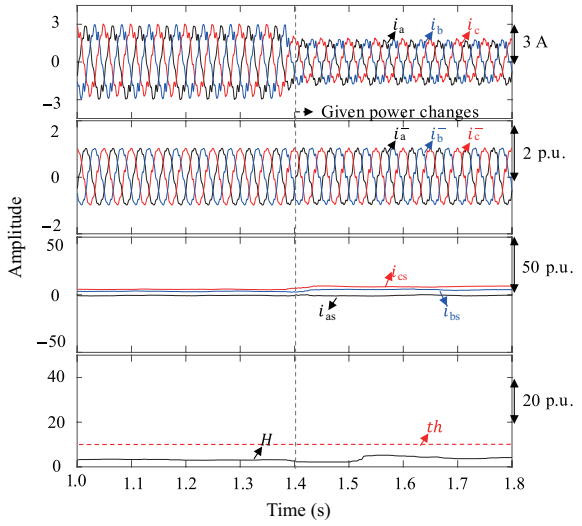

Fig. 7. Experimental results of changing given power.

Fig. 7 shows the performance verification with changing given power. The given current peak value is 3 A before 1.4 s, and 2 A at 1.4 s. The current normalization operation limits the three-phase current to the unit range in the whole process. The amplitudes of the currents decrease. However, i_{xs} and the Hausdorff distance H are all no significant changes, which also avoids the false trigger.

Fig. 8 shows the performance verification with changing DC source E. E is 300 V before 1.065 s, and 350 V at 1.065 s. The inverter takes a long time to reach a steady state. The current normalization operation limits the three-phase current to the unit range in the whole process. The amplitudes of the currents increase first and then decrease. However, i_{xs} and the Hausdorff distance H are all no significant changes, which also avoids the false trigger.

B. Fault Diagnosis Verification

Since the modulation index controls the action time of the switching state, it can be seen from Section III that modulation index regulation has an important impact on the current distortion under open-circuit fault. In this section, the size of E is changed to realize the modulation index regulation, and then the diagnostic effectiveness of the proposed method is verified.

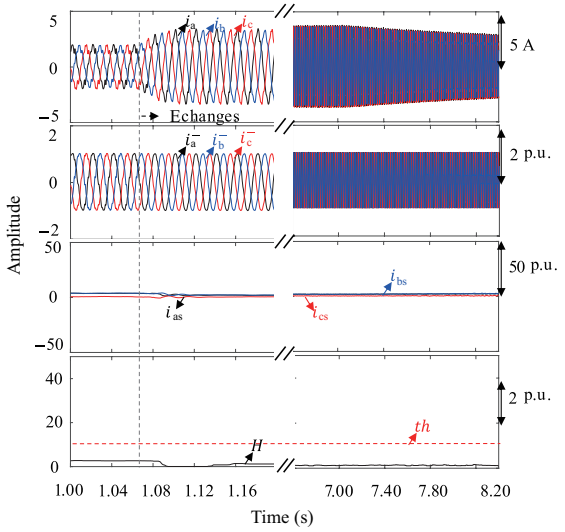

Fig. 8. Experimental results of changing DC source.

Fig. 9 shows the experimental results of S_{a1} fault with a modulation index of 0.8. Set S_{a1} fault at 1.14 s, and the positive period of i_a is distorted. The current normalization operation limits the three-phase current to the unit range in the whole process. The Hausdorff distance H is greater than th at about 1.185 s, and the fault is detected. After the fault is detected, $D_a < D_b < D_c$ and a-phase fault is detected. At the same time, $i_{as} < 0$ and $D_{an} < D_n$. Therefore, S_{a1}/S_{a3} fault is detected and S_{a1}/S_{a4} fault is detected. Finally, S_{a1} fault is correctly diagnosed.

Fig. 10 shows the experimental results of S_{a3} fault with modulation index 0.8. Set S_{a3} fault at 1.17 s, and the positive period of i_a is distorted. The current normalization operation limits the three-phase current to the unit range in the whole process. The Hausdorff distance H is greater than th at about 1.23 s, and the fault is detected. After the fault is detected, $D_a < D_b < D_c$ and a-phase fault is detected. At the same time, $i_{as} < 0$ and $D_{an} > D_n$. Therefore, S_{a1}/S_{a3} fault is detected and S_{a2}/S_{a3}fault is detected. Finally, S_{a3} fault is correctly diagnosed.

Fig. 11 shows the experimental results of S_{b1} fault with a modulation index being 0.2. With the decrease of the modulation index, the current distortion becomes more and more serious, which is consistent with the results of the analysis in Section III. The decrease in the modulation index increases the growth time of the negative current. The results of the proposed diagnosis in those experiments are the same as the experimental results at the modulation index of 0.8, which are correct. The average diagnosis time is about two current cycles.

Fig. 12 shows the experimental results of S_{a3} fault with a modulation index being 0.2. With the decrease of the modulation index, the current distortion becomes also more and more serious, which is consistent with the results of the

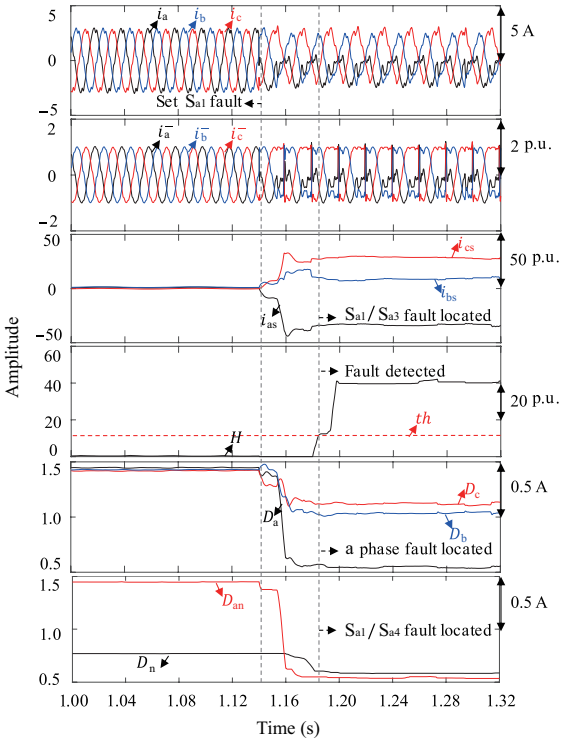

Fig. 9. Experimental results of S_{a1} fault with modulation index 0.8.

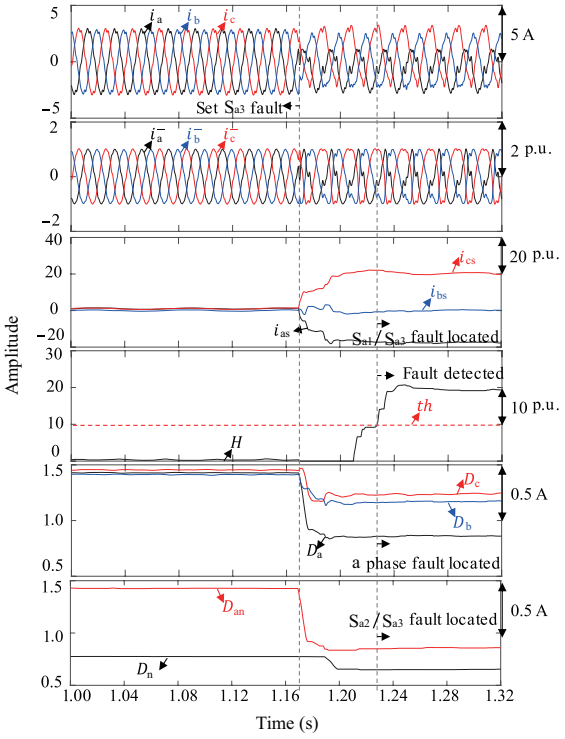

Fig. 10. Experimental results of S_{a3} fault with modulation index 0.8.

analysis in Section III. The decrease of the modulation index decreases the growth time of the positive current. The results of the proposed diagnosis in those experiments are the same as the experimental results at the modulation index of 0.8, which is correct. The average diagnosis time is about two current cycles.

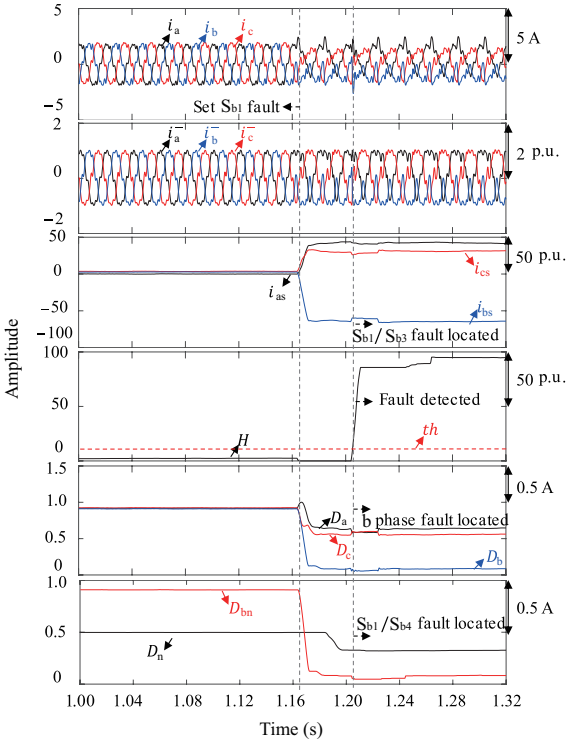

Fig. 11. Experimental results of S_{b1} fault with modulation index 0.2.

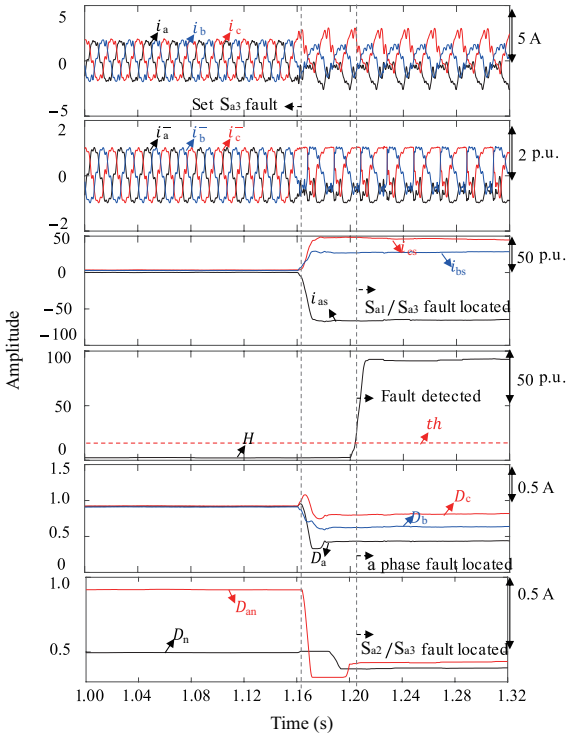

Fig. 12. Experimental results of S_{a3} fault with modulation index 0.2.

C. Compared With Previous Diagnosis Methods

The proposed method is compared with previous diagnosis methods as shown in Table II. The comparison indexes include diagnosis types, diagnosis variables, application objects, converter types, model dependence, cost, application range (whether to consider the modulation regulation, '*' represents

TABLE II
COMPARISON WITH PREVIOUS DIAGNOSIS METHODS

Method	Single/ Multiple fault	Diagnosis variable	Applicable objects	Converter type	Model dependence	Hardware/Calculation cost	Application range	Diagnostic time
[21]	Single	i_x, u_{xs}, switching state	Inverter (gird)	NPC	Low	No/Low	*	About 1.5 current cycles
[16]	Multiple	i_x	Inverter (RL)	NPC	Low	No/High	*	Less one current cycle
[13]	Single	V_{dc}, i_x, L_{xs}, u_{xs}, switching state and etc.	Rectifier	NPC	High	No/Low	*	Several switching periods
[20]	Single	i_x, power injection	Inverter (gird)	NPC	Low	No/Low	*	About 1.5 current cycles
[22]	Partial single	i_x, θ_x	Rectifier	T-type	Low	No/Low	*	About one current cycle
[12]	Single	i_x, u_{xs}, L_{xs}, U_{C1}, U_{C2}, U_{XN}, T_s, switching state and etc.	Inverter (RCL)	T-type	High	Yes/Low	Yes	Several switching periods
[23]	Single	Line voltage	Inverter (motor)	T-type	Low	Yes/High	*	About one current cycle
[24]	Single	i_x, i_n, switching state	Inverter (motor)	T-type	Low	Yes/Low	*	Several switching periods
[25]	Single	U_{C1}, U_{C2}, i_x	Inverter (RL)	T-type	Low	No/Low	*	About one current cycle
[11]	Single	U_{XN}, T_s, U_{C1}, U_{C2}, u_x, switching state	Inverter (RCL)	T-type	High	No/Low	Yes	About one current cycle
Proposed	Single	i_x	Inverter (gird)	T-type	Low	No/Low	Yes	About two current cycles

*, no validation

no validation), and diagnostic time. From the comparison, the advantages of the proposed method are: 1) Only the three-phase currents are needed for the diagnosis design, and the implemental cost of the proposed method is low. 2) The proposed method is suitable for all single transistor open-circuit faults, considering modulation index regulation.

VI. CONCLUSION

A novel online open-circuit fault diagnosis method for grid-tied T-type inverters based on only three-phase currents is proposed in this paper, which is suitable for all single transistor fault diagnosis. The distortion mechanism of the currents is analyzed in detail. The Hausdorff distances among the three-phase normalized current accumulations and the fundamental frequency values of the three-phase currents are used as diagnosis features. Compared with the existing methods, fewer system signals are used, which reduces the cost of diagnosis and the difficulty of implementation. Experimental results show the robustness under inverter transient conditions and effectiveness of fault diagnosis even with modulation index regulation.

REFERENCES

[1] A. Poorfakhraei, M. Narimani, and A. Emadi, "A review of multilevel inverter topologies in electric vehicles: current status and future trends," in *IEEE Open Journal of Power Electronics*, vol. 2, pp. 155–170, 2021.

[2] F. Blaabjerg, M. Liserre, and K. Ma, "Power electronics converters for wind turbine systems," in *IEEE Transactions on Industry Applications*, vol. 48, no. 2, pp. 708–719, Mar.-Apr. 2012.

[3] M. Schweizer and J. W. Kolar, "Design and implementation of a highly efficient three-level T-type converter for low-voltage applications," in *IEEE Transactions on Power Electronics*, vol. 28, no. 2, pp. 899–907, Feb. 2013.

[4] Z. Huang, D. Zhou, L. Wang, Z. Shen, and Y. Li, "A review of single-stage multiport inverters for multisource applications," in *IEEE Transactions on Power Electronics*, vol. 38, no. 5, pp. 6566–6584, May 2023.

[5] L. Alhmoud and B. Wang, "A review of the state-of-the-art in wind-energy reliability analysis," in *Renewable and Sustainable Energy Reviews*, Vol. 81, no. 2, pp. 1643–1651, Jan. 2018.

[6] B. Gou, X. Ge, S. Wang, X. Feng, J. B. Kuo, and T. G. Habetler, "An open-switch fault diagnosis method for single-phase PWM rectifier using a model-based approach in high-speed railway electrical traction drive system," in *IEEE Transactions on Power Electronics*, vol. 31, no. 5, pp. 3816–3826, May 2016.

[7] J. Falck, C. Felgemacher, A. Rojko, M. Liserre, and P. Zacharias, "Reliability of power electronic systems: An industry perspective," in *IEEE Industrial Electronics Magazine*, vol. 12, no. 2, pp. 24–35, Jun. 2018.

[8] Z. Yang and Y. Chai, "A survey of fault diagnosis for onshore grid-connected converter in wind energy conversion systems," in *Renewable and Sustainable Energy Reviews*, vol. 66, pp. 345–359, Dec. 2016.

[9] Z. Li, H. Ma, Z. Bai, Y. Wang, and B. Wang, "Fast transistor open-circuit faults diagnosis in grid-tied three-phase VSIs based on average bridge arm pole-to-pole voltages and error-adaptive thresholds," in *IEEE Transactions on Power Electronics*, vol. 33, no. 9, pp. 8040–8051, Sept. 2018.

[10] H. Zhang, C. Sun, Z. Li, J. Liu, H. Cao, and X. Zhang, "Voltage vector error fault diagnosis for open-circuit faults of three-phase four-wire active power filters," in *IEEE Transactions on Power Electronics*, vol. 32, no. 3, pp. 2215–2226, Mar. 2017.

[11] Y. Liang, R. Wang, and B. Hu, "Single-switch open-circuit diagnosis method based on average voltage vector for three-level T-Type inverter," in *IEEE Transactions on Power Electronics*, vol. 36, no. 1, pp. 911–921, Jan. 2021.

[12] B. Wang, Z. Li, Z. Bai, P. T. Krein, and H. Ma, "A voltage vector residual estimation method based on current path tracking for T-type inverter open-circuit fault diagnosis," in *IEEE Transactions on Power Electronics*, vol. 36, no. 12, pp. 13460–13477, Dec. 2021.

[13] L. M. A. Caseiro and A. M. S. Mendes, "Real-time IGBT open-circuit fault diagnosis in three-level neutral-point-clamped voltage-source rectifiers based on instant voltage error," in *IEEE Transactions on Industrial Electronics*, vol. 62, no. 3, pp. 1669–1678, Mar. 2015.

[14] Z. Huang, Z. Wang, and H. Zhang, "A diagnosis algorithm for multiple open-circuited faults of microgrid inverters based on main fault component analysis," in *IEEE Transactions on Energy Conversion*, vol. 33, no. 3, pp. 925–937, Sept. 2018.

[15] Y. Xia and Y. Xu, "A transferrable data-driven method for IGBT open-circuit fault diagnosis in three-phase inverters," in *IEEE Transactions on Power Electronics*, vol. 36, no. 12, pp. 13478–13488, Dec. 2021.

[16] W. Yuan, Z. Li, Y. He, R. Cheng, L. Lu, and Y. Ruan, "Open-circuit fault diagnosis of NPC inverter based on improved 1-D CNN network," in *IEEE Transactions on Instrumentation and Measurement*, vol. 71, pp. 1–11, 2022.

[17] F. Wu and J. Zhao, "A real-time multiple open-circuit fault diagnosis method in voltage-source-inverter fed vector controlled drives," in *IEEE Transactions on Power Electronics*, vol. 31, no. 2, pp. 1425–1437, Feb. 2016.

[18] N. M. A. Freire, J. O. Estima, and A. J. Marques Cardoso, "Open-circuit fault diagnosis in PMSG drives for wind turbine applications," in *IEEE Transactions on Industrial Electronics*, vol. 60, no. 9, pp. 3957–3967, Sept. 2013.

[19] X. Wu, C. -Y. Chen, T. -F. Chen, S. Cheng, Z. -H. Mao, T. -J. Yu, and K. Li, "A fast and robust diagnostic method for multiple open-circuit faults of voltage-source inverters through line voltage magnitudes analysis," in *IEEE Transactions on Power Electronics*, vol. 35, no. 5, pp. 5205–5220, May 2020.

[20] U. -M. Choi, J. -S. Lee, F. Blaabjerg, and K. -B. Lee, "Open-circuit fault diagnosis and fault-tolerant control for a grid-connected NPC inverter," in *IEEE Transactions on Power Electronics*, vol. 31, no. 10, pp. 7234–7247, Oct. 2016.

[21] U. -M. Choi, H. -G. Jeong, K. -B. Lee, and F. Blaabjerg, "Method for detecting an open-switch fault in a grid-connected NPC inverter system," in *IEEE Transactions on Power Electronics*, vol. 27, no. 6, pp. 2726–2739, Jun. 2012.

[22] J. -S. Lee and K. -B. Lee, "An open-switch fault detection method and tolerance controls based on SVM in a grid-connected T-type rectifier with unity power factor," in *IEEE Transactions on Industrial Electronics*, vol. 61, no. 12, pp. 7092–7104, Dec. 2014.

[23] K. -H. Chao, L. -Y. Chang, and F. -Q. Xu, "Three-level T-type inverter fault diagnosis and tolerant control using single-phase line voltage," in *IEEE Access*, vol. 8, pp. 44075–44086, 2020.

[24] J. He, N. A. O. Demerdash, N. Weise, and R. Katebi, "A fast on-line diagnostic method for open-circuit switch faults in SiC-MOSFET-based T-type multilevel inverters," in *IEEE Transactions on Industry Applications*, vol. 53, no. 3, pp. 2948–2958, May-Jun. 2017.

[25] U. -M. Choi, K. -B. Lee, and F. Blaabjerg, "Diagnosis and tolerant strategy of an open-switch fault for T-type three-level inverter systems," in *IEEE Transactions on Industry Applications*, vol. 50, no. 1, pp. 495–508, Jan.-Feb. 2014.

Zhixi Wu was born in Henan Province, China, in 1996. He received the B.S. degree in automation from Hunan University, Changsha, China, in 2018, and the M.S. degree in control science and engineering from Huazhong University of Science and Technology, Wuhan, China, in 2021. He is currently working toward the Ph.D. degree in artificial intelligence with the School of Artificial Intelligence and Automation, Huazhong University of Science and Technology. His research interests include multilevel converters and fault diagnosis for power converters.

Jin Zhao was born in Hubei Province, China, in 1967. He received the B.E. and Ph.D. degrees in Control Science and Engineering from the Department of Control Science and Engineering, Huazhong University of Science and Technology (HUST), Wuhan, China, in 1989 and 1994, respectively. Since 2004, he has been a Full Professor with the School of Artificial Intelligent and Automation, HUST. During 2001-2002, he was a Visiting Scholar in the Power Electronics Research Laboratory, University of Tennessee, Knoxville, USA. He is currently involved in research and applications of power electronics, electrical drives, fault diagnosis and tolerant, and intelligent control. He is the author or co-author of more than 300 technical papers.